pubs.acs.org/acschemicalbiology

Articles

Combined Effect of Anti-SSEA4 and Anti-Globo H Antibodies on Breast Cancer Cells

Ruey-Herng Lee, Yu-Jen Wang, Ting-Yen Lai, Tsui-Ling Hsu, Po-Kai Chuang, Han-Chung Wu, and Chi-Huey Wong*

Cite This: *ACS Chem. Biol.* 2021, 16, 1526−1537

Read Online

ACCESS | Metrics & More | Article Recommendations | Supporting Information

ABSTRACT: The globo-series glycosphingolipids (SSEA3, SSEA4, and Globo H) were shown to express in many cancers selectively, and a combination of anti-SSEA4 and anti-Globo H antibodies was able to suppress tumor growth in mice inoculated with breast cancer cell lines. To further understand the effect, we focused on the combined effect of the two antibodies in target binding and antibody-dependent cellular cytotoxicity (ADCC) in vitro. Here, we report that the binding of anti-Globo H antibody (VK9) to MDA-MB231 breast cancer cells was influenced by anti-SSEA4 antibody (MC813−70), and a combination of both antibodies induced a similar effect as did anti-SSEA4 antibodies alone in a reporter-based ADCC assay, indicating that SSEA4 is a major target in breast cancer due to its higher expression than Globo H. Furthermore, we showed that a homogeneous anti-SSEA4 antibody (chMC813−70-SCT) designed to maximize the ADCC activity can be used to isolate a subpopulation of natural killer (NK) cells that exhibit an ∼23% increase in killing the target cells as compared to the unseparated NK cells. These findings can be used to predict a therapy outcome based on the expression levels of antigens and evaluate therapeutic antibody development.

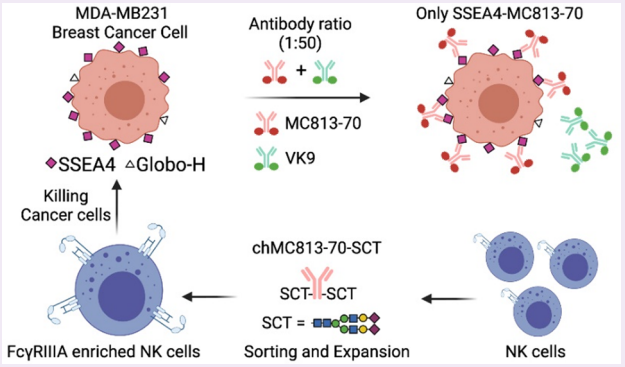

INTRODUCTION

Carbohydrates are often linked to lipids and proteins through glycosylation and expressed on a cell surface. They are involved in protein folding and many cellular recognition events.[1−3] However, the roles carbohydrates play in biology have not been well-understood until recently more advanced technology and more in-depth research have been reported, and their importance in biological processes has now been brought to light.[1]

Glycosphingolipids (GSLs) are the major glycolipids in the plasma membranes that consist of a glycan attached to a lipid moiety called ceramide. Variations in glycan and ceramide structures produce a tremendous diversity of GSLs, which are further classified into several series, such as ganglio, lacto, globo, etc.[2] GSL synthesis is initiated in the endoplasmic reticulum (ER) in which a sphingolipid base is condensed with an acyl-CoA to form a ceramide, which can be transported by ceramide transfer proteins (CERTs) to a trans-Golgi network (TGN) for the synthesis of sphingomyelin or by a vesicular transport to a cis-Glogi to generate glucosylceramide (GlcCer). GlcCer can then be transported either by another lipid transfer protein, a four-phosphate adaptor protein 2 (FAPP2), or by vesicular transport to the luminal leaflet of TGN, where GlcCer is galactosylated to form lactosylceramide (LacCer), which is further glycosylated with various glycosyltransferases in TGN to give different GSL series. Though the GSL expression is not template-driven, different cell types tend to exhibit a specific GSL expression. In fact, the GSL expression is strictly regulated during development and can serve as a cell-type-specific marker.[3] It was found that LacCer synthase (LCS) preferentially interacts with GM3 synthase (GM3S) in the Golgi cisternae, while it interacts with Gb3 synthase (Gb3S) in the TGN. On the one hand, if LacCer is transported via vesicular transport to the Golgi cisternae, it is primarily converted to ganglio-series GSLs. On the other hand, if LacCer is transported by FAPP2 to the TGN, it is converted to globo-series GSLs.[4]

GSLs tend to form a cluster in the lipid raft of the cell membrane and participate in various biological activities, including cell adhesion, proliferation, signaling, immune response, and infection. One study showed that the interaction between ganglioside GM3s can facilitate the adhesion and spreading of mouse melanoma B16 cell line.[5] Another study

Received: May 26, 2021
Accepted: July 27, 2021
Published: August 9, 2021

https://doi.org/10.1021/acschembio.1c00396
ACS Chem. Biol. 2021, 16, 1526−1537

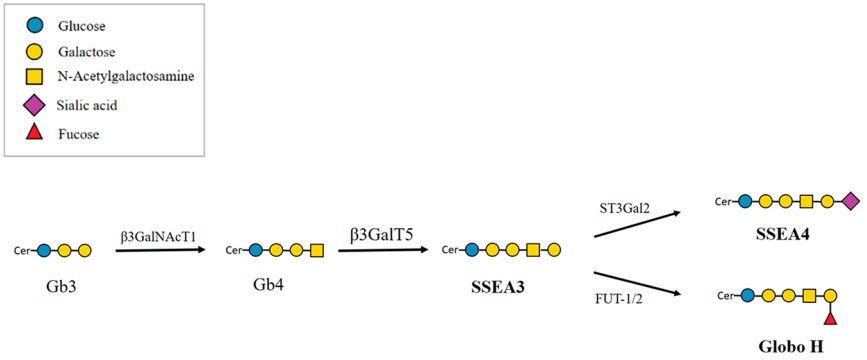

Figure 1. Biosynthesis of globo-series glycosphingolipids. Gb3, globotriaose; Gb4, globotetraose; SSEA3, stage-specific embryonic antigen 3; SSEA4, stage-specific embryonic antigen 4; β3GalNAcT1, β1,3-*N*-acetylgalactosaminyltransferase 1; β3GalT5, β1,3-galactosyltransferase V; ST3Gal-II, β-galactoside α2,3-sialyltransferase; FUT-1, fucosyltransferase-1; FUT-2, fucosyltransferase-2.

showed that GSLs can have an opposite effect: the ganglioside GD3 and globo-series Gb3 can inhibit a proliferation in the normal breast cell line MCF10A by activating the Merlin/NF2 tumor suppressor gene.[6] The fatty acid component of ceramide was found responsible for GSL signaling, and the metabolite sphingosine-1-phospate could induce an immune response.[7] LacCer can enhance neutrophils' phagocytosis of micro-organisms,[8] but many studies have shown that it is a target for some pathogens to infect cells.[9] As more and more biological functions of GSLs are uncovered, it is not surprising that GSL deregulation plays a role in human diseases. Indeed, the aberrant GSL expression has been observed in many neurological diseases as well as cancers. An overexpression of ganglioside GM1 in Alzheimer's disease was found to accelerate β-sheet formation of amyloide-β proteins.[10−12] In Parkinson's disease, however, the GM1 expression is much reduced.[13] Mice with Huntington's disease had an increased expression of GD1a and a reduced expression of GM2-Neu.[14] Ganglioside GD2 is overexpressed in a wide range of cancers and can activate signaling associated with proliferation, invasion, and motility. So far several anti-GD2 antibodies have been approved for clinical use.[15] More evidence has shown that ganglioside GD3 is a new potential target due to its ability to mediate tumor growth and high expression in many cancers.[16] Overall, the various biological functions of GSLs and their wide expression in human diseases have made GSLs a promising target in immunotherapy.

GLOBO-SERIES GSLS

Globo-series GSLs contain the basic structure globotriaose (Gb3) or Galα1,4Galβ1,4GlcCer. An addition of a β-linked *N*-acetylgalactosamine (GalNAc) to the terminal galactose of Gb3 generates globotetraose (Gb4). Galactosylation of Gb4 catalyzed by β1,3-galactosyltransferase V (β3GalT5) produces stage-specific embryonic antigen 3 (SSEA3), which serves as the precursor of SSEA4 and Globo H. A fucosylation of the terminal galactose of SSEA3 by fucosyltransferase-1 (FUT-1) and fucosyltransferase-2 (FUT-2) forms Globo H,[17] while the sialylation of a terminal galactose of SSEA3 by β-galactoside α2,3-sialyltransferase (ST3Gal-II) forms SSEA4 (Figure 1). SSEA3 and SSEA4 were originally observed on the pluripotent cells of the inner cell mass of a blastocyst during an early embryonic development, but they were lost upon differentiation. Therefore, scientists have used them to isolate human embryonic stem cells (hESCs). Other studies also showed that SSEA4 is expressed in stem cells from kidneys, testes, and ovaries.[18−20] Although the SSEA4 expression in normal cells is rare, it was found to increase rapidly in many cancers, including breast cancer,[21] basaloid lung cancer,[22] osteosarcoma,[23] prostate cancer,[24] ovarian cancer,[25] and oral cancer.[26] In addition, the anti-SSEA4 antibody MC813−70 was found to be able to trigger complement dependent cytotoxicity (CDC) in glioblastoma multiforme (GBM) cell lines expressing SSEA4 in vitro and inhibit the growth of a GBM cell line in a xenograft mouse model.[27] In addition to its broad expression in cancers, other studies have associated SSEA4 with characteristics of tumors, such as tumorigenicity, metastasis, and chemoresistance. $SSEA4^+$ osteosarcoma cells had a higher probability to form tumors in mice than $SSEA4^-$ cells.[23] $SSEA4^+$ prostate cancer downregulated epithelial-cell associated markers and upregulated mesenchymal markers, suggesting a gain of a migratory phenotype.[27] A high SSEA4 expression was observed in chemotherapy-resistant breast cancer cells and was correlated with a poor prognosis.[28]

In 1997, Globo H was found expressed in various epithelial cancers by immunohistochemistry, including small-cell lung, breast, prostate, pancreas, gastric, ovarian, and endometrial cancers. Also, because most breast cancer specimens have a Globo H expression and Globo H expressed by normal cells is extremely rare and inaccessible to the immune system, it has been considered as a promising target for immunotherapy and diagnosis.[17,29,30] Carbohydrates alone generally exhibit poor immunogenicity, so they are often conjugated with a carrier protein to induce a better immune response. It was shown that, when Globo H is conjugated to keyhole limpet hemocyanin (KLH) and adjuvanted with QS21 (a mixture of saponins), a strong immune response is induced to Globo H positive cancer cells. The vaccine was further developed by OBI for the treatment of triple-negative breast cancer, and a global phase 3 clinical trials is ongoing (NCT03562637).[31] It was also demonstrated that high IgG titers can be induced in mice when Globo H or SSEA4 is conjugated with Diphtheria toxoid (DT) and used as a vaccine in combination with an α-galactosylceramide analogue (C34) designed to act as an adjuvant and to induce a class switch from IgM to IgG.[21]

Previously, we found that SSEA3, SSEA4, and Globo H are overexpressed in GBM and various cancer cell lines of an additional 13 cancer types,[32] and SSEA3 and β3GalT5 are specific markers for breast cancer stem cells.[33] We also found that SSEA3, SSEA4, and Globo H form a complex in the lipid raft with caveolin-1 (CAV1) and focal adhesion kinase (FAK) for signaling.[34] Since SSEA4 and Globo H are expressed in

https://doi.org/10.1021/acschembio.1c00396
ACS Chem. Biol. 2021, 16, 1526−1537

most cancers, we hypothesized that targeting SSEA4 and Globo H simultaneously may be a better strategy (Figure 2).

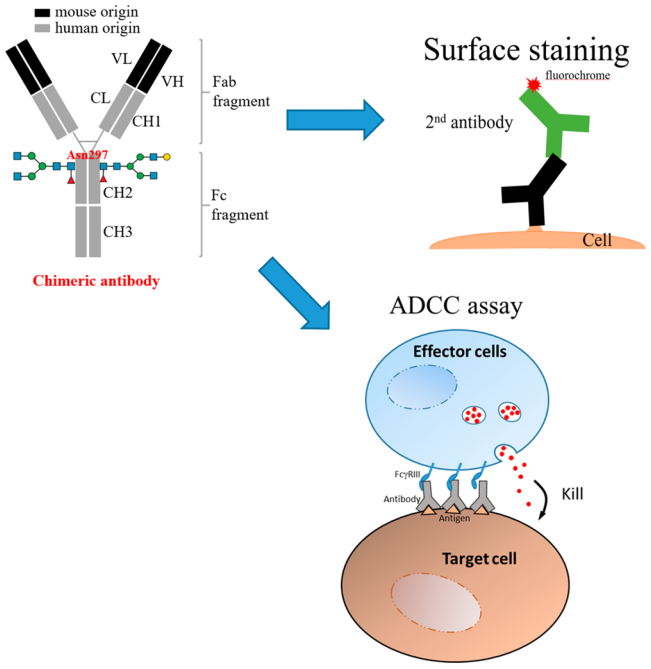

Figure 2. A schematic presentation of the research approach. To understand whether a synergistic effect[34] can be reproduced in vitro, we evaluated the combined effect of anti-SSEA4 and anti-Globo H antibodies by an ADCC assay and performed staining to detect the surface expression level of SSEA4 and Globo H as a reference. For surface staining, chimeric or mouse (not shown) antibodies were used. Antibody labeling for detection could be direct (not shown) or indirect. For an ADCC assay, only chimeric antibodies were used.

Preliminary data have shown that a combination using these two antibodies induced an additive or synergistic tumor suppression in mice.[34] Therefore, we would like to evaluate the combined effect of these two antibodies through an antibody-dependent cellular cytotoxicity (ADCC) assay to understand whether the effect observed in vivo could be reproduced in cell-based assays. Furthermore, by correlating the surface glycan staining with antibodies and their ADCC response, we can explore their use as a companion test to predict a therapy outcome based on patients' expression levels of globo-series GSLs as well as to evaluate strategies for therapeutic antibody development.

RESULTS

Surface Staining of Globo-Series GSLs. To understand the combined effect of anti-SSEA4 and anti-Globo H antibodies, it is essential to first understand whether they influence each other when binding to their antigens. Here we used certain concentrations of direct conjugated mouse antibodies, MC813−70 (anti-SSEA4) and VK9 (anti-Globo H), to perform single staining (with one type of antibody) and double staining (with two types of antibodies) on MCF-7 and MDA-MB-231. We hypothesize that, on the one hand, if the two antibodies do not influence each other in antigen binding, signals (mean florescence intensities relative to isotype control) from single staining and double staining should be similar. On the other hand, if they influence each other, signals from single staining and double staining should be different. For single staining, cells were incubated with 10 μg/mL MC813−70-AF488 or 5 μg/mL VK9-APC, both of which are oversaturated concentrations much greater than their K_D values (MC813−70: 4.21 ± 0.26 nM; VK9: 1 ± 0.116 nM).[30,32] For double staining, cells were incubated with an antibody mixture containing MC813−70-AF488 (10 μg/mL) and VK9-APC (5 μg/mL). After the flow cytometry analysis, we found that, for MC813−70, the single staining signal was comparable to the double staining signal on both cell lines, indicating that VK9 does not affect the antigen binding of MC813−70. For VK9, however, signals between single staining and double staining were different: MCF-7 had a lower signal in double staining, whereas MDA-MB-231 had a higher signal in double staining (hereinafter we refer to the difference as the VK9 signal difference). This suggests that MC813−70 can affect the antigen binding of VK9 (Figure 3a, Figure S1). This result prompted us to examine whether the VK9 signal difference also occurs in the double staining of SSEA3 and Globo H. Therefore, we double stained the two cell lines with MC631 (anti-SSEA3) and VK9. After three independent experiments, no significant VK9 signal difference was observed in both cell lines (Figure 3b), indicating that MC631 and VK9 do not influence each other in binding antigens.

Since mouse IgG3 antibodies have very low affinities to human FcγRIIIa receptor and thus induce a poor ADCC response, we obtained the chimeric antibodies chAb6 (anti-SSEA4 antibodies) and chVK9 (anti-Globo H antibodies) with a human IgG1 Fc portion, from Dr. HC Wu's laboratory, for the purpose of examining the ADCC response targeting SSEA4 and Globo H. First, we examined the combined effect of conjugated chAb6 and chVK9 by surface staining as well. The results showed that, similar to the double staining of SSEA4 and Globo H using mouse antibodies, chAb6 signals between single staining and double staining were similar. However, interestingly, chVK9 signals between single staining and double staining were also similar (Figure 3c). This indicates that chAb6 and chVK9 do not affect each other in antigen binding. We next used these two chimeric antibodies for a subsequent ADCC assay.

It is noteworthy that staining signals using conjugated antibodies are influenced by factors such as the fluorophore brightness and voltage setting on flow cytometers and, thus, do not reflect the actual or relative amounts of SSEA4 and Globo H. By a surface staining with unconjugated chimeric antibodies (indirect method) in the following experiments, the relative amount of SSEA4 and Globo H on MCF-7 is ∼10:1 (Figure 6, Table S3).

ChAb6 Induced a Higher ADCC Response than chVK9. To determine the ADCC response targeting SSEA4 and Globo H, we used chAb6 and chVK9, which share the same human IgG1 Fc sequence with a high affinity to human FcγRIIIa. Before evaluating a combined effect, we first tested these two antibodies separately on MCF-7, which has high levels of SSEA4 and Globo H expression among breast cancer cell lines. To measure the ADCC response, here we used an ADCC reporter bioassay, which has a lower variability and higher accuracy and precision than peripheral blood mononuclear cell (PMBC)-based ADCC. The results showed that chAb6 induced a more significant ADCC response than chVK9, indicating SSEA4 is probably a better target than Globo H in breast cancer. This difference in ADCC response was correlated with the difference in staining signal (by an indirect method) (Figure 4, Table S1).

https://doi.org/10.1021/acschembio.1c00396
ACS Chem. Biol. 2021, 16, 1526−1537

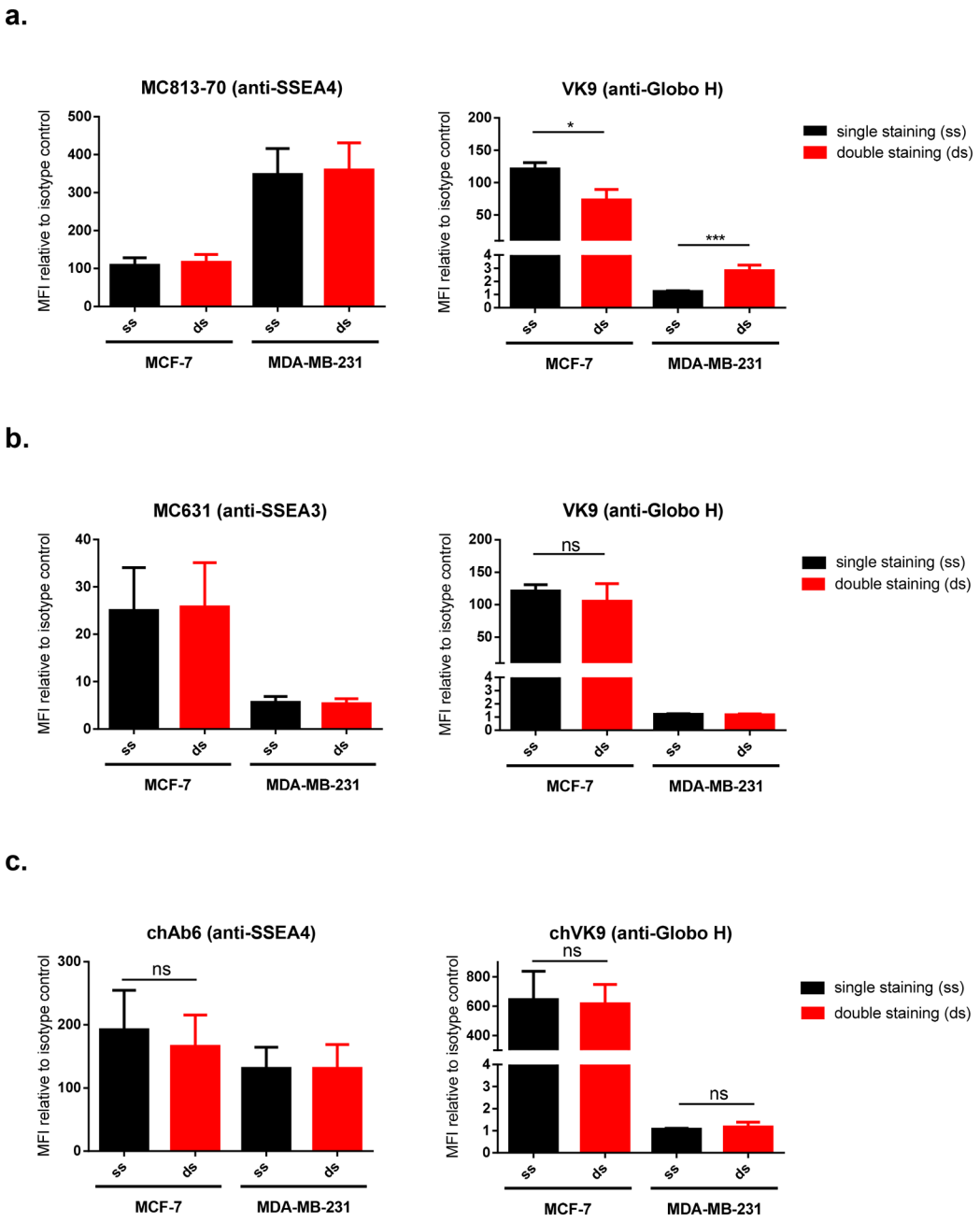

Figure 3. Surface staining of globo-series GSLs on MCF-7 and MDA-MB-231. (a) Double staining of SSEA4 and Globo H using AF488-conjugated MC813−70 and APC-conjugated VK9 (mouse antibodies). VK9 signal difference was observed: MCF-7 showed a reduced double staining signal, while MDA-MB-231 showed an increased double staining signal. This indicates that VK9 does not affect the antigen binding of MC813−70, but MC813−70 affects the antigen binding of VK9. The scatter plots are provided in Figure S1. (b) Double staining of SSEA3 and Globo H using AF488-conjugated MC631 and APC-conjugated VK9 (mouse antibodies). Single-staining and double-staining signals were similar for both MC631 and VK9, indicating the two antibodies do not affect each other when binding antigens. (c) Double staining of SSEA4 and Globo H using FITC-conjugated chAb6 and APC-conjugated chVK9 antibodies. Single-staining and double-staining signals were similar for both chAb6 and chVK9, indicating the two antibodies do not affect each other when binding antigens. To determine whether the two antibodies influence each other when binding antigens, we compared the staining signal mean fluorescence intensities (MFIs, representing the geometric mean intensities) relative to the isotype control between the single staining (ss, in black) and double staining (ds, in red) in each cell line.

To further understand the difference in the ADCC response, we checked the Fc glycosylation of these two antibodies, which could also affect the ADCC response. To this end, we digested the two antibodies with trypsin and subjected them to mass spectrometry for a glycoform analysis. The results showed that both antibodies have similar N-glycan compositions, with ~80% core-fucosylation and 42% with terminal galactosylation (Table 1). Compared with other glycan structures, FA2 and FA1 showed relatively different percentages between the two antibodies. However, these two glycan structures have not been reported to affect the ADCC response. We also noted that high mannose type N-glycans, which could reduce Fc core-fucosylation and thus increase the ADCC, are slightly different: chAb6 (7.93%) showed a somewhat higher percentage than chVK9 (4.79%). Overall, we concluded that

https://doi.org/10.1021/acschembio.1c00396
ACS Chem. Biol. 2021, 16, 1526−1537

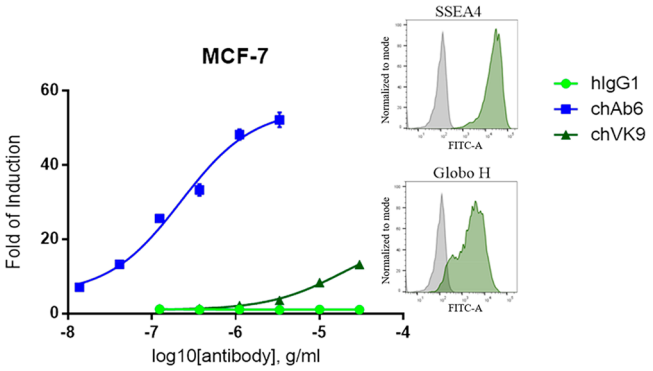

Figure 4. ADCC induction of chimeric Ab6 and chimeric VK9 and relative expression levels of SSEA4 and Globo H on MCF-7. ADCC assay was performed as described in Methods. The results showed that chAb6 induced a stronger ADCC response than chVK9 due to a high SSEA4 expression. Fold of induction is calculated as described in Methods. Surface staining was performed by an indirect method using 10 μg/mL unconjugated chAb6 or chVK9. The raw data are provided in Table S1.

the Fc glycosylation of these two antibodies may not contribute significantly to the ADCC response difference.

ChVK9 Induced Little ADCC Response. We then evaluated the combined effect of chAb6 and chVK9 by an ADCC assay in several breast cancer cell lines that were shown to express both SSEA4 and Globo H.[32] In combination groups, half the amount of each antibody was added so that the total amount of antibody is equal to that in single antibody groups. After 6 h of incubation with target cells and effector cells, the results showed that the combination groups induced a slightly lower ADCC response than chAb6 groups for each cell line (Figure 5 main graphs, Table S2). However, when we changed the *x*-axis from the total antibody concentration to the chAb6 concentration, the combination groups and chAb6 groups almost completely overlapped (Figure 5 inset graphs). This indicates that the ADCC response induced in the combination groups is primarily from chAb6. In other words, chVK9 hardly induced an ADCC response in combination. This phenomenon is particularly evident in Globo H$^+$ cell lines, MCF-7, and MDA-MB-157, in which chVK9 alone did induce an ADCC

Table 1. N-Glycan Compositions of Chimeric Ab6 and Chimeric VK9[a]

Symbol								
Name	A1	FA1	FA1G1	Hybrid	A2	FA2	A2G1	FA2G1
Symbol								
Name	A2G2	FA2G2	A2B	FA2B	A2BG1	High mannose		
						H5N2	H7N2	

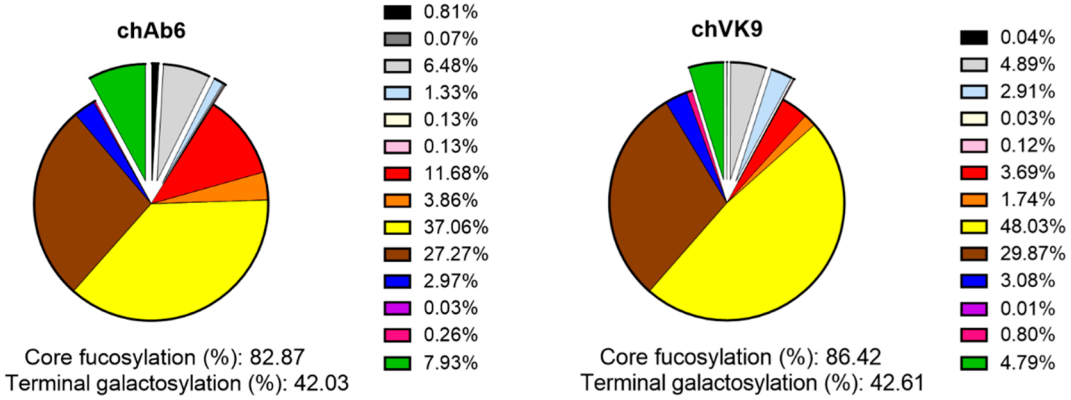

[a]ChAb6 and chVK9 were first digested by trypsin to produce glycopeptides (described in Methods) and then were analyzed for glycoforms by mass spectrometry. Non-core fucosylated N-glycans are shown as exploded slices. Numbers indicate the percentages of total N-glycan.

https://doi.org/10.1021/acschembio.1c00396
ACS Chem. Biol. 2021, 16, 1526−1537

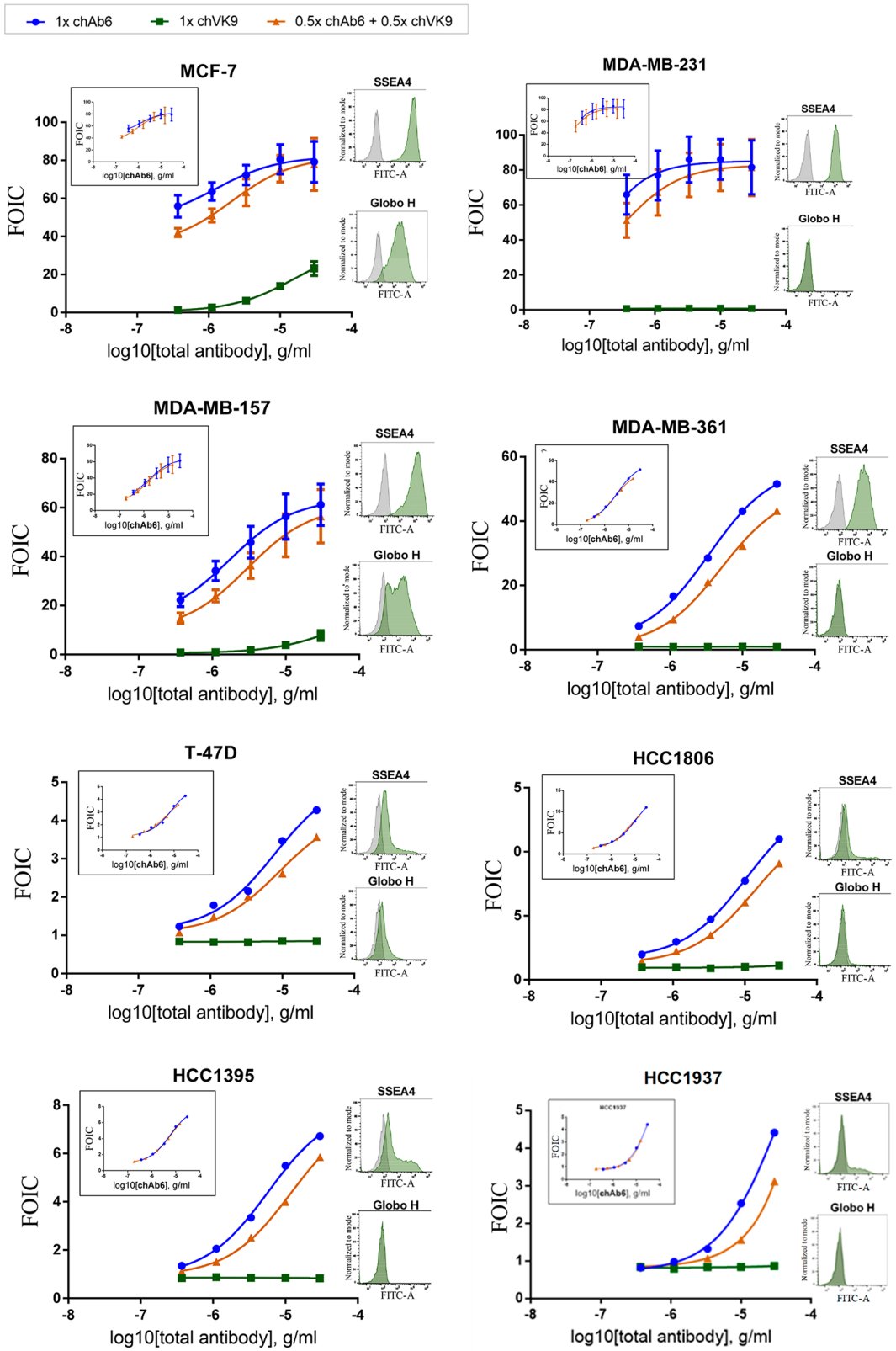

Figure 5. Combined effect of chAb6 and chVK9 in an ADCC assay on various breast cancer cell lines. In combination, half the amount of each antibody was added. The results showed that chAb6 induced most of the ADCC response in combination, whereas chVK9 induced very little. For the *y*-axis, FOIC stands for fold of induction (test/calibrator): Fold of induction (calculated as described in Methods) is divided by a common calibrator, in which 0.183 ng/mL Rituximab and WIL2-S (target cell) were used to compare between different cell lines. In the main graphs, the FOIC was plotted against the total antibody concentration. The inset graphs were generated by changing the *x*-axis to the chAb6 concentration. Surface staining was performed by an indirect method using 10 μg/mL unconjugated chAb6 or chVK9. The raw data are provided in Table S2.

https://doi.org/10.1021/acschembio.1c00396
ACS Chem. Biol. 2021, 16, 1526−1537

but did not induce a higher response in the combination groups.

Positive Correlation between Surface Expression and ADCC. For anti-SSEA4 and anti-Globo H antibodies to become therapeutic drugs, it is imperative to understand what specific groups of patients can benefit from this therapy, that is, how the expression levels of SSEA4 and Globo H are required to induce a significant ADCC response. Therefore, we correlated the staining signal with the ADCC response for each antibody concentration in each breast cancer cell line to create dot plots of SSEA4 and Globo H. Here we used the same batches of chAb6 and chVK9 for surface staining and ADCC assay to establish a better correlation. In surface staining, cells were first stained with these two antibodies, followed by a second incubation with AF488-conjugated goat antihuman IgG antibodies (described in Methods). The results showed that the SSEA4 dot plot exhibited a fitted curve, whereas the Globo H dot plot exhibited a fitted line (Figure 6, Table S3). In the SSEA4 dot plot, interestingly, MCF-7 and

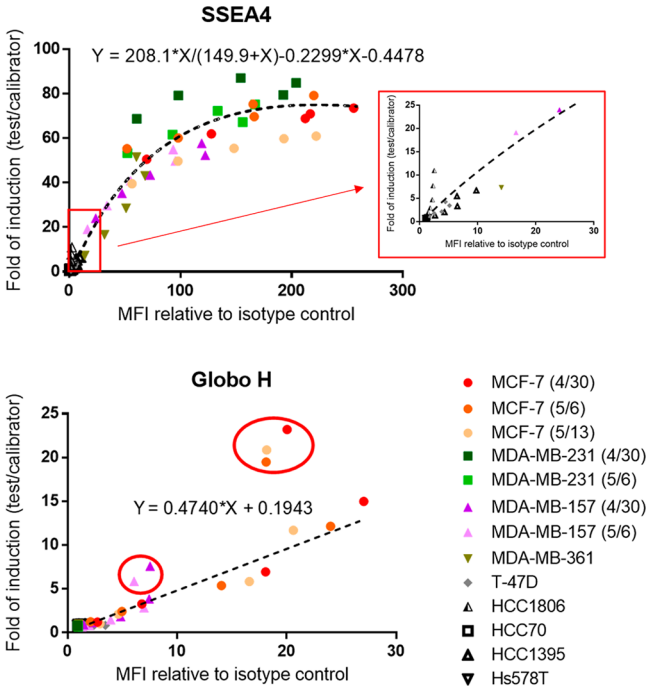

Figure 6. Correlation of staining signal with ADCC response on various breast cancer cell lines. SSEA4 and Globo H showed a positive correlation between the staining signal and the ADCC response. Surface staining was performed by an indirect method. Each point correlates one MFI relative to the isotype control with one-fold of induction for a single antibody concentration. Each symbol represents a breast cancer cell line, and different colors in each symbol represent independent experiments. An enlarged SSEA4 dot plot (in red box) is shown to compare with the Globo H dot plot. The best-fit line or curve was generated using GraphPad Prism 6 software. Points circled in red are indicated as outliers of the best-fit line, and for these points 30 μg/mL chVK9 was used. The raw data are provided in Table S3.

MDA-MB-231 exhibited slightly different correlations: For each antibody concentration, MCF-7 had a higher SSEA4 staining signal than MDA-MB-231, but it induced a lower ADCC response than MDA-MB-231. Next when we compared the two dot plots at the same scale, we found that, for each unit increase in staining signal, chAb6 induced an ADCC response more effectively than chVK9. Moreover, we noticed that, at 30 μg/mL chVK9, the staining signals were reduced, but ADCC responses remained increasing for MCF-7 and MDA-MB-157 (Figure 6).

We further study the competition between MC813−70 and VK9 by immunostaining. The cell-staining analysis showed that even MCF-7 cells, which have a high expression of Globo H, are predominantly bound with MC813−70 at the 1:50 ratio between MC813−70 and VK9 (Figure 7a). This is consistent with the surface staining results (Figure 3a). To further evaluate the therapeutic potential of anti-SSEA4 antibodies, we turned the commercially available and widely used anti-SSEA4 antibody MC813−70 into a homogeneous chimeric glycoform with 2,6-sialyl complex-type glycan attached to Asn-297 (chMC813−70-SCT, Figure 7b). On the basis of an SPR analysis and other structural studies, it was shown to enhance the avidity toward the FcγIIIA receptor and the corresponding ADCC effector function (Figure 7c).[35] This homogeneous antibody was then used to isolate a subpopulation of NK cells expressing FcγIIIA, and as expected the isolated NK cells showed an ∼23% increase in killing the target cells (MDA-MB-231) as compared to the unseparated NK cells (Figure 7d). This result reconfirms that an antibody such as MC813−70 with high avidity and specificity toward SSEA4 can be further transformed to a chimeric version to maximize its effector functions such as ADCC against target cells with a high expression of SSEA4 as demonstrated in this proof-of-concept study.

DISCUSSION

Though the combination of both antibodies induced a better effect in mice, we did not observe the effect in the ADCC cell-based assay. One possibility is that the ADCC assay we used measures an effector cell activation, which does not directly reflect cell death in mice. It is also possible that the better effect observed in mice resulted from a combination of multiple effects by other possible mechanisms, such as signaling or CDC or collective effects through targeting different individual cancer cells.

Since chAb6 and chVK9 have the same Fc region, similar glycoforms, and similar affinities to their antigens, the remarkable difference in the ADCC induction between chAb6 and chVK9 is due to their difference in staining signals. The surface staining of MCF-7 using unconjugated antibodies showed that, at the same antibody concentration, the chAb6 signal is ∼10 times higher than the chVK9 signal. Moreover, more than 95% of the cell population was labeled SSEA4$^+$ using 0.3 μg/mL chAb6, whereas chVK9 could only label as high as 80% of the cell population as Globo H$^+$, indicating that chAb6 stains cells more effectively than chVK9. There have been many reports that showed a strong correlation between the antigen expression level and the ADCC activity.[36,37] Therefore, we believe that SSEA4 is a better target than Globo H for therapeutic development due to its higher expression. Furthermore, a report showed that Siglec-7 and -9 ligands, sialic acid-containing carbohydrates, can inhibit a subpopulation of NK cells that bear Siglec-7 and -9 receptors.[38] If SSEA4, which also contains sialic acids, interacts with Siglec-7 and -9 receptors to suppress NK cell activities, anti-SSEA4 antibodies could block the interaction in addition to an ADCC induction. However, in the glycan array analysis, SSEA4 did not interact with Siglec-7 or Siglec-9.

The VK9 signal difference observed in the double staining of SSEA4 and Globo H using MC813−70 and VK9 is likely due

https://doi.org/10.1021/acschembio.1c00396
ACS Chem. Biol. 2021, 16, 1526−1537

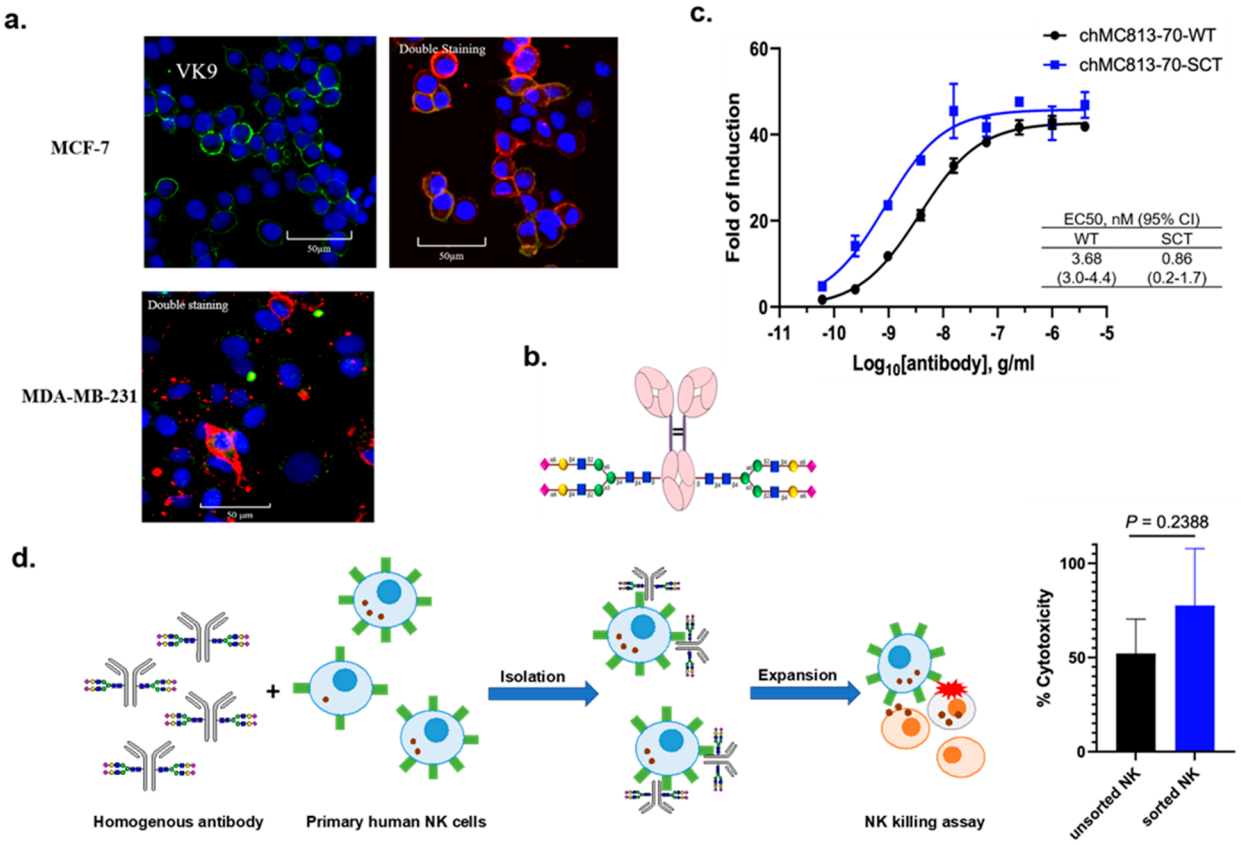

Figure 7. (a) Opera Phenix Image of MCF-7 and MDA-MB-231 breast cancer cells stained with FICT-conjugated VK9 (green, targeting Globo-H) only or with the mixture of APC-conjugated MC813−70 (red, targeting SSEA4) and FICT-conjugated VK9 in a 1:50 ratio (0.5 μg/mL: 25 μg/mL). The results showed that cells are still predominantly interacting with MC813−70. At a 1:1 ratio, the cancer cell is completely occupied by MC813−70. Nucleus is in blue (Hoechst 33342 (×1/500). (b) Homogeneous antibody MC813−70-SCT with maximized ADCC activity for the isolation of NK cells enriched with the FcγIIIA receptor responsible for the ADCC activity. (c) Comparison of heterogeneous and homogeneous chMC813−70 in an ADCC assay. The half-maximal effective concentrations (EC_{50}) for chMC813−70-WT were 3.68 ng/mL against MDA-MB-231, and for chMC813−70-SCT they were 0.86 ng/mL against MDA-MB-231. (d) Use of homogeneous antibody chMC813−70-SCT for isolation and expansion of a subpopulation of NK cells enriched with the FcγIIA receptor, which exhibited an ∼23% increase in killing the target cells (breast cancer cell line MDA-MB-231 with a high expression of SSEA4).

to steric hindrance. As noted in several studies, a steric hindrance can occur when antigens are closely spaced or when antibodies are conjugated to high molecular weight labels, such as ferritin (750 kDa) and phycoerythrin (250 kDa).[39,40] Here we demonstrated that allophycocyanin (APC) (105 kDa) does not lead to a steric hindrance because it, when conjugated to chVK9, did not significantly result in a chVK9 signal difference in the double staining of SSEA4 and Globo H using chAb6 and chVK9 (Figure 3c). Therefore, we suspected that SSEA4 is not only more expressed than Globo H but also is in close proximity to Globo H. This is further supported by the work of Chuang et al., which showed that globo-series GSLs formed a complex with CAV1 and FAK in the lipid raft to maintain a breast cancer cell survival.[34] Furthermore, we found that MC813−70 and chAb6 have different staining patterns in MCF-7 and MDA-MB-231 (Figure 3a,c), and both antibodies as well as VK9 have a similar avidity to their antigens with K_d in the nanomolar range, suggesting that chAb6 and MC813−70 may bind to SSEA4 differently.

The cross-linking of Fc receptors is a critical step in triggering effector cell activation. It occurs when antibodies bind to antigens, in a soluble form or on a cancer cell surface, to form immune complexes, which then bring Fc receptors together to induce signaling in immune cells.[41] For example, FcγRIIIa cross-linking can induce an intracellular calcium mobilization and trigger a degranulation in NK cells.[42,43] In addition to an antigen expression level, we suspected that the antigen distribution may affect the level of FcγRIIIa cross-linking. The observation that the anti-SSEA4 antibody is more effective at inducing an ADCC than anti-Globo H antibody is probably due to the higher density of SSEA4 that enhances the FcγRIIIa cross-linking. Also, slightly different correlations of MCF-7 and MDA-MB-231 in an SSEA4 dot plot (Figure 6) and staining signal differences between SSEA4 and Globo H suggest that distributions and densities of SSEA4 and Globo H on cell surfaces between different breast cancer cell lines are different. Apart from an antigen expression level and distributions, characterizing the avidity of chAb6 and chVK9 antibodies to antigens and FcγRIIIa can help further understand an ADCC response and different correlation on each cell line.

In the correlation experiment, when the chVK9 concentration reaches 30 μg/mL, we observed a reduced staining signal but a significantly higher ADCC response in MCF-7 and MDA-MB-157. We speculate that a high antibody concentration might result in an antibody aggregation, in which the Fc region of the antibody can still bind to FcγRIIIa (CD16a), while the Fab region is not bound to antigens. FcγRIIIa is a

https://doi.org/10.1021/acschembio.1c00396
ACS Chem. Biol. 2021, 16, 1526−1537

low-affinity Fc receptor that has been reported to be able to bind aggregated IgGs and increase the ADCC response.[44,45] However, if antibodies are aggregated due to oxidation or other reactions that destabilize their structures, the ADCC response will significantly decrease.[46,47]

In our study, we found that expression levels of SSEA4 and Globo H were heterogeneous in various breast cancer cell lines. Thus, an examination of the expression levels of these two antigens on breast cancer cells is necessary to determine the effectiveness of SSEA4- and Globo H-targeted therapy for patients. Apart from the correlation data (Figure 6), circulating tumor cells (CTCs) could also be examined for a therapy assessment. CTCs are cells that are shed from the primary tumor and enter the circulatory system, which enables them to form a new tumor in a distant tissue. Recent studies have demonstrated that CTCs contribute to breast cancer metastasis and are indicative of worse survival in breast cancer patients.[48,49] They can even provide a quiescent population of the tumor that could be the cause of a treatment resistance. One such example is that CTCs from human epidermal growth factor receptor 2 (HER2)-negative^{-} patients were found to be HER2-positive.[50] Thanks to a technology advancement, breast CTCs now can be detected with a high efficiency and purity.[51,52] Overall, we can stain patients' CTCs to examine expression levels of SSEA4 and Globo H and determine whether they are eligible for the targeted therapy or vaccination.

In conclusion, our results suggested that SSEA4 is a better target than Globo H in breast cancer due to its higher expression and that the antigen distribution and density may play a role in an ADCC induction. The establishment of the correlation between a staining signal and an ADCC response can help assess the therapy effectiveness for patients and evaluate strategies for therapeutic antibody development.

METHODS

Cell Culture. Breast cancer cell lines were obtained from the American Type Culture Collection (ATCC). MCF-7 was maintained in RPMI 1640 supplemented with 10% (v/v) fetal bovine serum (FBS) and 1X non-essential amino acid (NEAA). MDA-MB-231 and T-47D were maintained in Dulbecco's Modified Eagle's Medium (DMEM) supplemented with 10% (v/v) FBS. MDA-MB-361 was maintained in DMEM/F12 with 10% FBS. Other breast cancer cell lines were cultured according to the ATCC. FBS supplemented with 5% dimethyl sulfoxide (DMSO) was used as a freeze medium in cryopreservation.

Production of Chimeric VK9 Antibodies. Chimeric VK9 plasmids were obtained from Institute of Cellular and Organismic Biology, Academia Sinica. The plasmid transformation was performed using HIT DH5α, followed by a plasmid extraction (QIAGEN plasmid MEGA kit). The Expi293F expression system (Thermo Fisher Scientific) was used to express chimeric VK9. Antibody purification was performed on ÄKTA start (GE Healthcare Life Sciences) using HiTrap Protein A HP column (1 mL, GE Healthcare Life Sciences), followed by a desalting using two HiTrap Desalting columns (5 mL, GE Healthcare Life Sciences) in series to exchange buffer to 1X phosphate-buffered saline (PBS).

For the plasmid transformation, 500 ng of light-chain or heavy-chain plasmids was incubated with 100 μL of HIT DH5α on ice for 10 min. Ten microliters of the mixture containing plasmids and HIT DH5α along with 100 μL of luria broth (LB) was plated onto a prewarmed LB agar plate containing 100 μg/mL ampicillin. Plating beads were used to spread the mixture across the plate surface, and the plate was then incubated in the incubator at 37 °C. For the plasmid extraction, after centrifugation at 6000g for 15 min at 4 °C, bacterial cell pellets were sequentially treated with a resuspension buffer, lysis buffer, and neutralization buffer to extract plasmid DNAs, which were then purified using an anion-exchange resin column. After they were precipitated, washed, and air-dried, plasmid DNAs were dissolved in Tris ethylenediaminetetraacetic acid (TE) buffer and stored at 4 °C.

After the transfection, the transfection supernatant was first centrifuged at 8000 rpm for 15 min at 4 °C and filtered through a 0.22 nm filter. An HiTrap Protein A HP column and HiTrap Desalting columns were washed with deionized water and 1X PBS before use. For the antibody purification, an HiTrap Protein A HP column was equilibrated with 2 mL of 1X PBS for 30 s. During a sample loading, the supernatant passed through the column at 4 mL/min for 2 h 10 min, followed by a wash with 20 mL of 1X PBS. The bound chVK9 was then eluted with pH 3 glycine and neutralized with pH 9.1 M Tris/HCl. (Tris/HCl-to-glycine ratio = 1:15). The eluents containing chVK9 were combined and subjected to desalting. Two HiTrap Desalting columns were equilibrated with 5 mL of 1X PBS for 1 min. During a sample loading, the flow rate was set to 1 mL/min, and 5 mL of 1X PBS was used to elute chVK9 for 5 min.

Antibody Glycoform Analysis by in-Solution Tryptic Digestion. First, 7.5 μL of a digestion buffer (50 mM ammonium bicarbonate) and 0.75 μL of 100 mM reducing buffer (100 mM dithiolthreitol) were added to 10 μL (2 μg) of an antibody sample. The mixture was adjusted to 18.5 μL with ultrapure water and incubated at 95 °C for 5 min. Next, 1.5 μL of alkylation buffer (100 mM iodoacetamide) was added to the sample and allowed to react in the dark at room temperature (RT) for 20 min. After the alkylation, the sample was treated with 1 μL of trypsin (0.4 μg/μL) and was placed in the incubator at 37 °C overnight. After 12−16 h, the sample was heated to 95 °C for 10 min and subjected to mass spectrometry.

For the glycoform analysis, the signal for each glycan structure was normalized to a percentage of the total signals. Glycan structures were further organized based on the presence of fucoses or galactoses to determine percentages of core-fucosylation and terminal galactosylation.

Surface Staining and Flow Cytometry. (a) Staining with direct conjugated mouse antibodies. In a single staining, 0.5 μg of Alexa Fluor 488 (AF488)-conjugated anti-SSEA4 mAb (MC813−70), 0.5 μg of Alexa Fluor 488 (AF488)-conjugated anti-SSEA3 mAb (MC631), or 0.25 μg of allophycocyanin (APC)-conjugated anti-Globo H mAb (VK9) was used to stain 2 × 10^5 cells in 50 μL of fluorescence-activated cell sorting (FACS) buffer (1X PBS with 1% FBS) for 30 min at 4 °C in the dark. In a double staining, 0.5 μg of AF488-conjugated MC813−70 or 0.5 μg of AF488-conjugated MC631 was mixed with 0.25 μg of APC-conjugated VK9 prior to staining 2 × 10^5 cells. (b) Staining with direct conjugated chimeric antibodies. In a single staining, 0.5 μg of fluorescein isothiocyanate (FITC)-conjugated anti-SSEA4 chimeric mAb (chAb6) or 0.5 μg of APC-conjugated anti-Globo H chimeric mAb (chVK9) was used to stain 2 × 10^5 cells in 50 μL of FACS buffer for 30 min at 4 °C in the dark. In double staining, 0.5 μg of FITC-conjugated chAb6 was mixed with 0.5 μg of APC-conjugated chVK9 prior to staining 2 × 10^5 cells. After 30 min of incubation at 4 °C in the dark, cells were washed twice with 200 μL of FACS buffer and then were resuspended with 200 μL of FACS buffer containing 1 μg/mL propidium iodide (PI) before a flow cytometry analysis. The data acquisition was performed using FACSCanto (BD Biosciences), and data were analyzed by FlowJo (BD Biosciences). (c) Staining with unconjugated chimeric antibodies (indirect method). Cells (2 × 10^5) were incubated with five concentrations of unconjugated chAb6 or chVK9 (30, 10, 3.33, 1.11, 0.37 μg/mL) in 50 μL of FACS buffer for 30 min. After the primary incubation, cells were washed with 150 μL of FACS buffer and centrifuged at 500g for 3 min to discard supernatants. For the secondary incubation, cells were incubated with 50 μL of FACS buffer containing 1 μg/mL Alexa Fluor 488 (AF488)-conjugated goat antihuman IgG antibodies for 30 min at 4 °C in the dark before a flow cytometry analysis. Data acquisition was performed using FACSCanto (BD Biosciences), and data were analyzed by FlowJo (BD Biosciences).

https://doi.org/10.1021/acschembio.1c00396
ACS Chem. Biol. 2021, 16, 1526−1537

ADCC Reporter Bioassay. An ADCC reporter bioassay (Promega G7014) was performed using engineered Jurkat cells expressing the human FcγRIIIa-V158 receptor. Multiple cross-linking of target cells with Jurkat cells by antibodies leads to Jurkat cell luciferase production, which can be quantified to determine the Jurkat cell activation. Target cells were seeded at 12 500 cells per well in a 96-well white plate and incubated at 37 °C, 5% CO_2 overnight. After 12−16 h, serial dilutions of antibodies were first added to target cells; 75 000 Jurkat cells were then added to the wells already containing target cells and antibodies. The effector cell/target cell (E/T) ratio was 6:1. After 6 h of incubation at 37 °C and 5% CO_2, the plate was allowed to cool to RT for 15 min, followed by an addition of a luciferase substrate. Five minutes after the luciferase substrate addition, the luminescence was measured using CLARIOstar (BMG Labtech). The fold of induction was calculated by dividing relative light unit (RLU) (induced-background) by RLU (no antibody control-background). GraphPad Prism 6 software was used for the data analysis.

Immunofluororescence Microscopy. Cells were seeded in 96-well plates, cultured for 1 d, and rinsed with PBS followed by a fixation with 4% paraformaldehyde/PBS at RT for 30 min and PBS rinse. After they were blocked with 5% bovine serum albumin (BSA)/PBS for 30 min, FICT-conjugated VK9 and APC-conjugated MC813−70 antibodies were added in either a 1:1 (0.5 μg/mL:0.5 μg/mL) or 1:50 ratio (0.5 μg/mL:25 μg/mL) for double staining or FICT-conjugated VK9 alone (0.5 or 25 μg/mL) for single staining. Nuclei of cells were stained with Hoechst 33342 (10 μg/mL) for 10 min followed by a PBS rinse. Stained cells were mounted by 50% glycerol/PBS and subjected to Opera Phenix for image acquisition.

Primary Human NK Cell Culture and Ex Vivo Expansion of Isolated NK Cells. Cryopreserved primary human NK cells were purchased from Cellero. The homogeneous antibody chMC813−70-SCT with a 2,6-sialyl complex-type glycan (SCT) attached to Asn-297 was prepared according to the procedure described previously[50] was used to sort the NK cells for expansion. We used NK MACS Medium (Miltenyi Biotec) with 5% human AB serum (Sigma-Aldrich) and 500 U/mL Interleukin 2 (IL-2) to culture the NK cells. A DNase I treatment (10 U/mL) is necessary to prevent cell aggregation and death after thawing. Afterward, we utilized the NK killing assay to measure the NK cytotoxicity. Briefly, NK cells were treated with IL-2 (500 U/mL) for expansion and stained with chMC81370-SCT-conjugated FITC and sorted by FACSAriaIIU (BD Biosciences). The sorted NK cells were resuspended in an NK MACS medium system containing 500 U/mL IL-2 and then incubated at 37 °C, 5% CO_2.

Analysis of the Primary NK Cells Cytotoxicity Via NK Killing Assay. An NK killing assay was performed using the LDH-Glo Cytotoxicity Assay. The target cells (5000 cells/100 μL) were seeded into a 96-well flat-bottom microplate overnight. The RPMI Medium with 0.5% human AB serum and IL-2 (500 U/mL) was used as the NK killing assay buffer. Then the effector cells (NK cells) in a 10:1 E/T ratio were added to the 96-well flat-bottom microplate, and the cells were incubated for additional 4 h at 37 °C, 5% CO_2. After the incubation, the mixture was transferred to another 96-well microplate and 100 times diluted by a lactate dehydrogenase (LDH) storage buffer. The diluted mixture of 50 μL and the LDH-detection buffer of 50 μL were mixed together. The microplate was incubated at RT for 1 h, and the luminescence was read by the CLARIOstar. The data were calculated, and the statistical analyses were performed using GraphPad Prism software. The unpaired *t* test was used to test for a statistical significance in the NK killing assay. The percentage of target cells lysis was calculated according to the CDC assay formula: percentage of cell lysis = (luminescence of the experimental − luminescence of background)/(luminescence of the maximum − luminescence of background) × 100.

■ ASSOCIATED CONTENT

Supporting Information

The Supporting Information is available free of charge at https://pubs.acs.org/doi/10.1021/acschembio.1c00396.

Scatterplots and raw data (PDF)

■ AUTHOR INFORMATION

Corresponding Author

Chi-Huey Wong − *Genomics Research Center, Academia Sinica, Taipei 115, Taiwan; Department of Chemistry, The Scripps Research Institute, La Jolla, California 92037, United States;* orcid.org/0000-0002-9961-7865; Email: wong@scripps.edu

Authors

Ruey-Herng Lee − *Genomics Research Center, Academia Sinica, Taipei 115, Taiwan; Department of Chemistry, National Taiwan University, Taipei 106, Taiwan;* Present Address: Ruey-Herng Lee, Tanvex Biologics Corporation, 33F, No. 99, Section 1, Xintai 5th Road, Xizhi District, New Taipei City 221, Taiwan

Yu-Jen Wang − *Genomics Research Center, Academia Sinica, Taipei 115, Taiwan; Institute of Biochemical Sciences, National Taiwan University, Taipei 106, Taiwan*

Ting-Yen Lai − *Genomics Research Center, Academia Sinica, Taipei 115, Taiwan*

Tsui-Ling Hsu − *Genomics Research Center, Academia Sinica, Taipei 115, Taiwan*

Po-Kai Chuang − *Department of Chemistry, The Scripps Research Institute, La Jolla, California 92037, United States*

Han-Chung Wu − *Institute of Cellular and Organismic Biology, Academia Sinica, Taipei 115, Taiwan*

Complete contact information is available at: https://pubs.acs.org/10.1021/acschembio.1c00396

Notes

The authors declare no competing financial interest.

■ ACKNOWLEDGMENTS

We are grateful for all the materials and assistance from M. Hsiao (GRC, Academia Sinica). We thank Glycan Sequencing Core at GRC, Academia Sincia, for the glycoform profiling. We also thank the Core Facilities of Translational Medicine of BioTReC (National Biotechnology Research Park, Academic Sinica) for the fluorescence imaging and data analysis. This research was supported by Academia Sinica Summit Program, NIH (AI-130227), and NSF (CHE-1954031).

■ REFERENCES

(1) Krasnova, L.; Wong, C. H. Oligosaccharide Synthesis and Translational Innovation. *J. Am. Chem. Soc.* **2019**, *141*, 3735−3754.

(2) Schnaar, R. L., Suzuki, A., Stanley, P. (2009) Glycosphingolipids. In *Essentials of Glycobiology*, 2nd ed., Cold Spring Harbor Laboratory Press.

(3) D'Angelo, G.; Capasso, S.; Sticco, L.; Russo, D. Glycosphingolipids: synthesis and functions. *FEBS J.* **2013**, *280*, 6338−6353.

(4) D'Angelo, G.; Uemura, T.; Chuang, C.-C.; Polishchuk, E.; Santoro, M.; Ohvo-Rekilä, H.; Sato, T.; Di Tullio, G.; Varriale, A.; D'Auria, S. Vesicular and non-vesicular transport feed distinct glycosylation pathways in the Golgi. *Nature* **2013**, *501*, 116.

(5) Kojima, N.; Hakomori, S.-i. Synergistic effect of two cell recognition systems: glycosphingolipid-glycosphingolipid interaction and integrin receptor interaction with pericellular matrix protein. *Glycobiology* **1991**, *1*, 623−630.

(6) Huang, X.; Schurman, N.; Handa, K.; Hakomori, S. Functional role of glycosphingolipids in contact inhibition of growth in a human mammary epithelial cell line. *FEBS Lett.* **2017**, *591*, 1918−1928.

(7) Iwabuchi, K., Nakayama, H., Oizumi, A., Suga, Y., Ogawa, H., Takamori, K. (**2015**) Role of ceramide from glycosphingolipids and its metabolites in immunological and inflammatory responses in humans, *Mediators Inflammation 2015*.1
(8) Nakayama, H.; Yoshizaki, F.; Prinetti, A.; Sonnino, S.; Mauri, L.; Takamori, K.; Ogawa, H.; Iwabuchi, K. Lyn-coupled LacCer-enriched lipid rafts are required for CD11b/CD18-mediated neutrophil phagocytosis of nonopsonized microorganisms. *J. Leukocyte Biol.* **2008**, *83*, 728−741.
(9) Karlsson, K.-A. Animal glycolipids as attachment sites for microbes. *Chem. Phys. Lipids* **1986**, *42*, 153−172.
(10) Kakio, A.; Nishimoto, S.; Yanagisawa, K.; Kozutsumi, Y.; Matsuzaki, K. Interactions of amyloid beta-protein with various gangliosides in raft-like membranes: importance of GM1 ganglioside-bound form as an endogenous seed for Alzheimer amyloid. *Biochemistry* **2002**, *41*, 7385−7390.
(11) Ikeda, K.; Yamaguchi, T.; Fukunaga, S.; Hoshino, M.; Matsuzaki, K. Mechanism of amyloid beta-protein aggregation mediated by GM1 ganglioside clusters. *Biochemistry* **2011**, *50*, 6433−6440.
(12) Yagi-Utsumi, M.; Matsuo, K.; Yanagisawa, K.; Gekko, K.; Kato, K. Spectroscopic Characterization of Intermolecular Interaction of Amyloid beta Promoted on GM1Micelles. *Int. J. Alzheimer's Dis.* **2011**, *2011*, 925073.
(13) Wu, G.; Lu, Z. H.; Kulkarni, N.; Ledeen, R. W. Deficiency of ganglioside GM1 correlates with Parkinson's disease in mice and humans. *J. Neurosci. Res.* **2012**, *90*, 1997−2008.
(14) Gizaw, S. T.; Koda, T.; Amano, M.; Kamimura, K.; Ohashi, T.; Hinou, H.; Nishimura, S. A comprehensive glycome profiling of Huntington's disease transgenic mice. *Biochim. Biophys. Acta, Gen. Subj.* **2015**, *1850*, 1704−1718.
(15) Suzuki, M.; Cheung, N. K. Disialoganglioside GD2 as a therapeutic target for human diseases. *Expert Opin. Ther. Targets* **2015**, *19*, 349−362.
(16) Liu, J.; Zheng, X.; Pang, X.; Li, L.; Wang, J.; Yang, C.; Du, G. Ganglioside GD3 synthase (GD3S), a novel cancer drug target. *Acta Pharm. Sin. B* **2018**, *8*, 713−720.
(17) Chang, W. W.; Lee, C. H.; Lee, P.; Lin, J.; Hsu, C. W.; Hung, J. T.; Lin, J. J.; Yu, J. C.; Shao, L. E.; Yu, J.; Wong, C.-H.; Yu, A. L. Expression of Globo H and SSEA3 in breast cancer stem cells and the involvement of fucosyl transferases 1 and 2 in Globo H synthesis. *Proc. Natl. Acad. Sci. U. S. A.* **2008**, *105*, 11667−11672.
(18) Rahman, M. S.; Spitzhorn, L. S.; Wruck, W.; Hagenbeck, C.; Balan, P.; Graffmann, N.; Bohndorf, M.; Ncube, A.; Guillot, P. V.; Fehm, T.; Adjaye, J. The presence of human mesenchymal stem cells of renal origin in amniotic fluid increases with gestational time. *Stem. Cell. Res. Ther.* **2018**, *9*, 113.
(19) Harichandan, A.; Sivasubramaniyan, K.; Hennenlotter, J.; Schwentner, C.; Stenzl, A.; Buhring, H. J. Isolation of adult human spermatogonial progenitors using novel markers. *J. Mol. Cell Biol.* **2013**, *5*, 351−353.
(20) Virant-Klun, I.; Skutella, T.; Hren, M.; Gruden, K.; Cvjeticanin, B.; Vogler, A.; Sinkovec, J. Isolation of small SSEA-4-positive putative stem cells from the ovarian surface epithelium of adult human ovaries by two different methods. *BioMed Res. Int.* **2013**, *2013*, 690415.
(21) Huang, Y. L.; Hung, J. T.; Cheung, S. K.; Lee, H. Y.; Chu, K. C.; Li, S. T.; Lin, Y. C.; Ren, C. T.; Cheng, T. J.; Hsu, T. L.; Yu, A. L.; Wu, C. Y.; Wong, C. H. Carbohydrate-based vaccines with a glycolipid adjuvant for breast cancer. *Proc. Natl. Acad. Sci. U. S. A.* **2013**, *110*, 2517−2522.
(22) Gottschling, S.; Jensen, K.; Warth, A.; Herth, F. J.; Thomas, M.; Schnabel, P. A.; Herpel, E. Stage-specific embryonic antigen-4 is expressed in basaloid lung cancer and associated with poor prognosis. *Eur. Respir. J.* **2013**, *41*, 656−663.
(23) Zhang, W.; Ding, M. L.; Zhang, J. N.; Qiu, J. R.; Shen, Y. H.; Ding, X. Y.; Deng, L. F.; Zhang, W. B.; Zhu, J. mTORC1 maintains the tumorigenicity of SSEA-4(+) high-grade osteosarcoma. *Sci. Rep.* **2015**, *5*, 9604.
(24) Nakamura, Y.; Miyata, Y.; Matsuo, T.; Shida, Y.; Hakariya, T.; Ohba, K.; Taima, T.; Ito, A.; Suda, T.; Hakomori, S. I.; Saito, S.; Sakai, H. Stage-specific embryonic antigen-4 is a histological marker reflecting the malignant behavior of prostate cancer. *Glycoconjugate J.* **2019**, *36*, 409−418.
(25) Virant-Klun, I.; Kenda-Suster, N.; Smrkolj, S. Small putative NANOG, SOX2, and SSEA-4-positive stem cells resembling very small embryonic-like stem cells in sections of ovarian tissue in patients with ovarian cancer. *J. Ovarian Res.* **2016**, *9*, 12.
(26) Noto, Z.; Yoshida, T.; Okabe, M.; Koike, C.; Fathy, M.; Tsuno, H.; Tomihara, K.; Arai, N.; Noguchi, M.; Nikaido, T. CD44 and SSEA-4 positive cells in an oral cancer cell line HSC-4 possess cancer stem-like cell characteristics. *Oral Oncol.* **2013**, *49*, 787−795.
(27) Sivasubramaniyan, K.; Harichandan, A.; Schilbach, K.; Mack, A. F.; Bedke, J.; Stenzl, A.; Kanz, L.; Niederfellner, G.; Buhring, H. J. Expression of stage-specific embryonic antigen-4 (SSEA-4) defines spontaneous loss of epithelial phenotype in human solid tumor cells. *Glycobiology* **2015**, *25*, 902−917.
(28) Aloia, A.; Petrova, E.; Tomiuk, S.; Bissels, U.; Deas, O.; Saini, M.; Zickgraf, F. M.; Wagner, S.; Spaich, S.; Sutterlin, M.; Schneeweiss, A.; Reitberger, M.; Ruberg, S.; Gerstmayer, B.; Agorku, D.; Knobel, S.; Terranegra, A.; Falleni, M.; Soldati, L.; Sprick, M. R.; Trumpp, A.; Judde, J. G.; Bosio, A.; Cairo, S.; Hardt, O. The sialyl-glycolipid stage-specific embryonic antigen 4 marks a subpopulation of chemotherapy-resistant breast cancer cells with mesenchymal features. *Breast Cancer Res.* **2015**, *17*, 146.
(29) Zhang, S.; Cordon-Cardo, C.; Zhang, H. S.; Reuter, V. E.; Adluri, S.; Hamilton, W. B.; Lloyd, K. O.; Livingston, P. O. Selection of tumor antigens as targets for immune attack using immunohistochemistry: I. Focus on gangliosides. *Int. J. Cancer* **1997**, *73*, 42−49.
(30) Wang, C. C.; Huang, Y. L.; Ren, C. T.; Lin, C. W.; Hung, J. T.; Yu, J. C.; Yu, A. L.; Wu, C. Y.; Wong, C.-H. Glycan microarray of Globo H and related structures for quantitative analysis of breast cancer. *Proc. Natl. Acad. Sci. U. S. A.* **2008**, *105*, 11661−11666.
(31) Danishefsky, S. J.; Shue, Y. K.; Chang, M. N.; Wong, C. H. Development of Globo-H cancer vaccine. *Acc. Chem. Res.* **2015**, *48*, 643−652.
(32) Lou, Y. W.; Wang, P. Y.; Yeh, S. C.; Chuang, P. K.; Li, S. T.; Wu, C. Y.; Khoo, K. H.; Hsiao, M.; Hsu, T. L.; Wong, C.-H. Stage-specific embryonic antigen-4 as a potential therapeutic target in glioblastoma multiforme and other cancers. *Proc. Natl. Acad. Sci. U. S. A.* **2014**, *111*, 2482−2487.
(33) Cheung, S. K.; Chuang, P. K.; Huang, H. W.; Hwang-Verslues, W. W.; Cho, C. H.; Yang, W. B.; Shen, C. N.; Hsiao, M.; Hsu, T. L.; Chang, C. F.; Wong, C.-H. Stage-specific embryonic antigen-3 (SSEA-3) and beta3GalT5 are cancer specific and significant markers for breast cancer stem cells. *Proc. Natl. Acad. Sci. U. S. A.* **2016**, *113*, 960−965.
(34) Chuang, P. K.; Hsiao, M.; Hsu, T. L.; Chang, C. F.; Wu, C. Y.; Chen, B. R.; Huang, H. W.; Liao, K. S.; Chen, C. C.; Chen, C. L.; Yang, S. M.; Kuo, C. W.; Chen, P.; Chiu, P. T.; Chen, I. J.; Lai, J. S.; Yu, C. T.; Wong, C.-H. Signaling pathway of globo-series glycosphingolipids and beta1,3-galactosyltransferase V (beta3GalT5) in breast cancer. *Proc. Natl. Acad. Sci. U. S. A.* **2019**, *116*, 3518−3523.
(35) Lin, C. W.; Tsai, M. H.; Li, S. T.; Tsai, T. I.; Chu, K. C.; Liu, Y. C.; Lai, M. Y.; Wu, C. Y.; Tseng, Y. C.; Shivatare, S. S.; Wang, C. H.; Chao, P.; Wang, S. Y.; Shih, H. W.; Zeng, Y. F.; You, T. H.; Liao, J. Y.; Tu, Y. C.; Lin, Y. S.; Chuang, H. Y.; Chen, C. L.; Tsai, C. S.; Huang, C. C.; Lin, N. H.; Ma, C.; Wu, C. Y.; Wong, C.-H. A common glycan structure on immunoglobulin G for enhancement of effector functions. *Proc. Natl. Acad. Sci. U. S. A.* **2015**, *112*, 10611−10616.
(36) Seo, Y.; Ishii, Y.; Ochiai, H.; Fukuda, K.; Akimoto, S.; Hayashida, T.; Okabayashi, K.; Tsuruta, M.; Hasegawa, H.; Kitagawa, Y. Cetuximab-mediated ADCC activity is correlated with the cell surface expression level of EGFR but not with the KRAS/BRAF mutational status in colorectal cancer. *Oncol. Rep.* **2014**, *31*, 2115−2122.
(37) Velders, M. P.; van Rhijn, C. M.; Oskam, E.; Fleuren, G. J.; Warnaar, S. O.; Litvinov, S. V. The impact of antigen density and

https://doi.org/10.1021/acschembio.1c00396
ACS Chem. Biol. 2021, 16, 1526−1537

antibody affinity on antibody-dependent cellular cytotoxicity: relevance for immunotherapy of carcinomas. *Br. J. Cancer* **1998**, *78*, 478−483.
(38) Jandus, C.; Boligan, K. F.; Chijioke, O.; Liu, H.; Dahlhaus, M.; Demoulins, T.; Schneider, C.; Wehrli, M.; Hunger, R. E.; Baerlocher, G. M.; Simon, H. U.; Romero, P.; Munz, C.; von Gunten, S. Interactions between Siglec-7/9 receptors and ligands influence NK cell-dependent tumor immunosurveillance. *J. Clin. Invest.* **2014**, *124*, 1810−1820.
(39) Kent, S. P.; Ryan, K. H.; Siegel, A. L. Steric hindrance as a factor in the reaction of labeled antibody with cell surface antigenic determinants. *J. Histochem. Cytochem.* **1978**, *26*, 618−621.
(40) De Vita, M.; Catzola, V.; Buzzonetti, A.; Fossati, M.; Battaglia, A.; Zamai, L.; Fattorossi, A. Unexpected interference in cell surface staining by monoclonal antibodies to unrelated antigens. *Cytometry, Part B* **2014**, *88*, 352−354.
(41) Lu, L. L.; Suscovich, T. J.; Fortune, S. M.; Alter, G. Beyond binding: antibody effector functions in infectious diseases. *Nat. Rev. Immunol.* **2018**, *18*, 46−61.
(42) Bryceson, Y. T.; March, M. E.; Ljunggren, H. G.; Long, E. O. Synergy among receptors on resting NK cells for the activation of natural cytotoxicity and cytokine secretion. *Blood* **2006**, *107*, 159−166.
(43) Bhatnagar, N.; Ahmad, F.; Hong, H. S.; Eberhard, J.; Lu, I. N.; Ballmaier, M.; Schmidt, R. E.; Jacobs, R.; Meyer-Olson, D. FcgammaRIII (CD16)-mediated ADCC by NK cells is regulated by monocytes and FcgammaRII (CD32). *Eur. J. Immunol.* **2014**, *44*, 3368−3379.
(44) Lopez, E.; Scott, N. E.; Wines, B. D.; Hogarth, P. M.; Wheatley, A. K.; Kent, S. J.; Chung, A. W. Low pH Exposure During Immunoglobulin G Purification Methods Results in Aggregates That Avidly Bind Fcgamma Receptors: Implications for Measuring Fc Dependent Antibody Functions. *Front. Immunol.* **2019**, *10*, 2415.
(45) Geuijen, K. P. M.; Oppers-Tiemissen, C.; Egging, D. F.; Simons, P. J.; Boon, L.; Schasfoort, R. B. M.; Eppink, M. H. M. Rapid screening of IgG quality attributes - effects on Fc receptor binding. *FEBS Open Bio* **2017**, *7*, 1557−1574.
(46) Shah, D. D.; Zhang, J.; Hsieh, M. C.; Sundaram, S.; Maity, H.; Mallela, K. M. G. Effect of Peroxide- Versus Alkoxyl-Induced Chemical Oxidation on the Structure, Stability, Aggregation, and Function of a Therapeutic Monoclonal Antibody. *J. Pharm. Sci.* **2018**, *107*, 2789−2803.
(47) Shah, D. D.; Zhang, J.; Maity, H.; Mallela, K. M. G. Effect of photo-degradation on the structure, stability, aggregation, and function of an IgG1 monoclonal antibody. *Int. J. Pharm.* **2018**, *547*, 438−449.
(48) Aceto, N.; Bardia, A.; Miyamoto, D. T.; Donaldson, M. C.; Wittner, B. S.; Spencer, J. A.; Yu, M.; Pely, A.; Engstrom, A.; Zhu, H.; Brannigan, B. W.; Kapur, R.; Stott, S. L.; Shioda, T.; Ramaswamy, S.; Ting, D. T.; Lin, C. P.; Toner, M.; Haber, D. A.; Maheswaran, S. Circulating tumor cell clusters are oligoclonal precursors of breast cancer metastasis. *Cell* **2014**, *158*, 1110−1122.
(49) Bidard, F. C.; Vincent-Salomon, A.; Sigal-Zafrani, B.; Dieras, V.; Mathiot, C.; Mignot, L.; Thiery, J. P.; Sastre-Garau, X.; Pierga, J. Y. Prognosis of women with stage IV breast cancer depends on detection of circulating tumor cells rather than disseminated tumor cells. *Ann. Oncol.* **2008**, *19*, 496−500.
(50) Riethdorf, S.; Muller, V.; Zhang, L.; Rau, T.; Loibl, S.; Komor, M.; Roller, M.; Huober, J.; Fehm, T.; Schrader, I.; Hilfrich, J.; Holms, F.; Tesch, H.; Eidtmann, H.; Untch, M.; von Minckwitz, G.; Pantel, K. Detection and HER2 expression of circulating tumor cells: prospective monitoring in breast cancer patients treated in the neoadjuvant GeparQuattro trial. *Clin. Cancer Res.* **2010**, *16*, 2634−2645.
(51) Wang, G.; Benasutti, H.; Jones, J. F.; Shi, G.; Benchimol, M.; Pingle, S.; Kesari, S.; Yeh, Y.; Hsieh, L. E.; Liu, Y. T.; Elias, A.; Simberg, D. Isolation of Breast cancer CTCs with multitargeted buoyant immunomicrobubbles. *Colloids Surf., B* **2018**, *161*, 200−209.
(52) Loeian, M. S.; Mehdi Aghaei, S.; Farhadi, F.; Rai, V.; Yang, H. W.; Johnson, M. D.; Aqil, F.; Mandadi, M.; Rai, S. N.; Panchapakesan, B. Liquid biopsy using the nanotube-CTC-chip: capture of invasive CTCs with high purity using preferential adherence in breast cancer patients. *Lab Chip* **2019**, *19*, 1899−1915.

https://doi.org/10.1021/acschembio.1c00396
ACS Chem. Biol. 2021, 16, 1526−1537